Journal of Food Engineering 339 (2023) 111277

Contents lists available at ScienceDirect

Journal of Food Engineering

journal homepage: www.elsevier.com/locate/jfoodeng

Improving 3D food printing performance using computer vision and feedforward nozzle motion control

Yizhou Ma [a], Jelle Potappel [a], Aneesh Chauhan [b], Maarten A.I. Schutyser [a], Remko M. Boom [a], Lu Zhang [a,*]

[a] Laboratory of Food Process Engineering, Wageningen University and Research, P.O. Box 16, 6700, AA, Wageningen, the Netherlands
[b] Wageningen Food and Biobased Research, Bornse Weilanden 9, P.O. Box 17, 6700, AA, Wageningen, the Netherlands

ARTICLE INFO

Keywords:
3D food printing
Die swell
Optical flow
Food rheology
Computer vision

ABSTRACT

3D food printing is an emerging technology to customize food designs and produce personalized foods. Food printing materials are diverse in rheological properties, which makes reliable extrusion-based 3D printing with constant printing parameters a challenge. Food printing often suffers from improper extrusion because of the varying elasticity of the food materials. In this study, a computer vision (CV)-based method is developed to measure the instant extrusion rate and width under constant extrusion pressure/force. The measured extrusion rate and extruded filament width were used to conduct a feedforward control of nozzle motion for a pneumatic 3D food printer. As a result, the CV-based control method improves extrusion line accuracy to 97.6–100% and prevents under-extrusion of white chocolate spread, cookie dough, and processed cheese. The method can also be used to customize filament width with less than 8% of deviation from the target. With a simple measurement setup and a user-friendly software interface, this CV-based method is deployable to most food printing applications to reduce trial-and-error experiments when printing a new food material.

1. Introduction

Extrusion-based 3D printing is the most common technique for food printing. It relies on deposition of a viscoelastic food material through a nozzle to build 3D food structures layer by layer. Food materials such as chocolate, cookie dough, protein dispersions, and hydrocolloid gels have been successfully printed into customized shapes that may tailor to specific consumer preferences (Hao et al., 2010; Liu et al., 2019a, 2019b; Montoya et al., 2021; Sun et al., 2020). The flavor and texture of 3D printed foods can be customized by changing the spatial distribution of flavorings and controlling the geometric designs (Zhu et al., 2020, 2021), offering an advantage over mass produced foods (Derossi et al., 2021). More recently, 4D food printing applications were developed to create dynamic changes of color, shape, and flavor of 3D printed foods (Teng et al., 2021). Over the last 14 years, food researchers have gained insights about food material printability, printing material formulations, and printing parameter optimizations, with the aim to produce personalized foods in the future (Derossi et al., 2021).

3D printing of chocolate has already been successfully applied in food manufacturing due to chocolate's popularity among consumers and the development of specialized chocolate printers to ensure high product quality. The commercial chocolate printers can print manufacturer-optimized "chocolate inks" with a set of pre-determined settings provided by the manufacturer. However, unlike chocolate, other food materials do not have customized printers to streamline the printing process for high-quality printed foods. Currently, extrusion-based food printers are mostly modified units of fused deposition modelling printers and pneumatic bioprinters (Wegrzyn et al., 2012). Extensive trial-and-error experiments are still needed to determine the proper printing parameters for a given food material due to the large variations in the viscoelastic properties of food materials (Siacor et al., 2021).

One of the common defects in extrusion-based 3D food printing is under- or over-extrusion of filaments due to improper extrudability and the creation of a "die swell" (i.e. expanded extruded filament width) by food materials (Fahmy et al., 2020a). The extrudability and die swell of food materials are governed by various factors. Specifically, the extrusion temperature, pressure, nozzle geometry, and material properties have been identified as factors to determine the extrudability of food materials with complex formulations (Ma et al., 2021). Over-extrusion is specifically related to die-swell of polymeric food materials due to stress

* Corresponding author.
E-mail address: lu1.zhang@wur.nl (L. Zhang).

https://doi.org/10.1016/j.jfoodeng.2022.111277
Received 1 July 2022; Received in revised form 25 August 2022; Accepted 5 September 2022
Available online 8 September 2022

relaxation and is influenced by the printing pressure and the length of the printing nozzle (Le-Bail et al., 2020). To compensate for under- and over-extrusion during food printing, the nozzle motion should synchronize with the filament's instant extrusion rate (Wu et al., 2021). Therefore, determining the instant extrusion rate and extruded filament width of food materials may allow the optimization of the nozzle motion parameters to reduce the 3D food printing defects. The determination of instant extrusion rate (i.e. flow rate profile) and filament width could be achieved by either computer simulation or experimental measurement.

Computational fluid dynamic (CFD) modelling has been applied to predict the extrusion rate and optimize the printing processes for plastics (Moretti et al., 2021; Serdeczny et al., 2020b; Xia et al., 2018). The pressure drop and heat transfer models were resolved using rheological and thermal properties of the plastic materials. This approach can predict the extrusion flow and material solidification in a fixed extruder design (Xia et al., 2018). CFD modelling was subsequently applied to optimize the nozzle motion, improve printing accuracies, and design more efficient extruders in thermoplastic printing applications (Comminal et al., 2019; Ertay et al., 2018). However, simulating extrusion flow is computationally resourceful and requires extensive quantification of the material's physical properties. Therefore, the CFD modelling approach is best suited to provide fundamental understanding of the printing process and optimize printer designs for materials that are well understood and characterized (Go et al., 2017). In food printing, CFD modelling has not yet been widely applied due to the variations of the physical properties of foods leading to tedious simulation development and limited predictability because of the changing material properties. One study attempted to simulate the distributions of velocity, shear rate and pressure of food materials inside of a printing syringe using material rheological properties and syringe geometry (Liu et al., 2020a, 2020b). It highlighted the dynamics of the material extrusion process but did not provide an applicable control strategy. A different study simulated the velocity distribution in a food printing nozzle using the continuity equations of volume transfer, assuming a constant extrusion rate and incompressibility of the food materials (Guo et al., 2020). This estimation could therefore only provide indications of the performance at steady state but cannot be used to minimize dynamic under- and over-extrusion.

An alternative to computer simulation is in-situ measurement. To determine the instant extrusion rate of plastic materials, optical methods based on computer vision (CV) have been used. The Lucas-Kanade optical flow algorithm was applied in several studies to determine the extrusion rates of plastic filament (Greeff and Schilling, 2017; Moretti et al., 2021). A close-up camera can film the filament extruding from the nozzle, and the optical flow analysis tracks the pixel intensity changes on the filament, identifies the filament's movement, and calculate its instant velocity. This approach has provided experimental support for numerical simulations and allowed closed-loop controls of 3D plastic printing to prevent filament slippage (Greeff and Schilling, 2017). Using a similar optical method, a different study developed an extruded filament width measurement tool based on computer vision (Tian et al., 2021). It used the instant extruded filament width to correct for printing inconsistencies during extrusion printing of polydimethyl siloxane (PDMS). Currently, the extrusion flow rate and extruded filament width measurements are mostly used for experimental validation and in-situ monitoring purposes. Besides simply monitoring the flow of materials, the quantitative data acquired via CV-based measurements may also be used to optimize printing parameters to achieve more consistent printing quality. In food printing, extensive trial-and-error experiments are often needed to understand the material extrudability, because printing materials are diverse and have complex rheological properties (Ma et al., 2021). To expedite the parameter tuning process of printing complex food materials, a CV-based measurement of instant flow rate can provide a helpful control strategy which leads to proper extrusion consistency and improved printing accuracy.

This study therefore aims to develop and evaluate a feedforward control method based on CV to improve the printing accuracy of complex food materials. Briefly, a CV-based tracking method was developed as a calibration step to measure the extrusion rate and extruded filament width of common food printing materials. The nozzle motion (i.e. nozzle moving velocity) was calibrated based on the measured instant extrusion rate and extruded filament width. The calibrated nozzle motion was then implemented to evaluate its effectiveness from two aspects: 1) extrusion latency compensation and 2) customized extrusion width. The calibrated nozzle motions were compared to the results with constant nozzle motion to demonstrate the improved printing accuracy.

2. Materials and methods

2.1. Printing materials

White chocolate spread (Albert Heijn, the Netherlands), lemon curd (Chivers, the Netherlands), dry cookie dough mix (Dawn Foods, the United States), and processed cheese (ERU, the Netherlands) were purchased from a local supermarket (Albert Heijn, the Netherlands). The cookie dough was prepared according to the manufacturer's instruction: 100 g of the dry cookie dough mix was combined with 14 g of butter and 9 g of water and mixed for 20 min using a kitchen mixer. The food materials were kept at 4 °C and tempered to 20 °C before use. Ingredient lists of food materials used in this study are included in Appendix A.

In the subsequent sections, the white chocolate spread and lemon curd were used to develop and validate the extrusion rate measurement method based on CV. The white chocolate spread and processed cheese were used to develop the extruded filament width measurement technique. After the methods were established, a series of calibrated motion controls were demonstrated using white chocolate spread, cookie dough, and processed cheese. The lemon curd was not used for printing demonstrations due to its large variations in extrusion rate measured from the method development phase. In the end of the study, processed cheese was printed into a complicated shape to demonstrate the performance improvement in a real printing application.

2.2. Printing material characterizations

To characterize the rheological properties of the materials, frequency sweeps were performed following the method of Zhang et al. (2020). Briefly, a rheometer equipped with a 20-mm cone and plate geometry (2° angle) was used (Anton Paar Physica MCR502, Anton Paar GmbH, Graz, Austria). The angular frequency was increased from 0.1 to 100 rad/s, and the corresponding storage and loss moduli were recorded to examine viscoelastic properties at the corresponding printing temperatures (20 or 50 °C).

To characterize the surface roughness of the extruded materials, they were carefully transferred into a syringe (⌀ 22 mm, Optimum Syringe Barrel, Nordson EFD, USA) connected to a dispensing nozzle with internal diameters varying between 0.84 and 1.54 mm (Nordson EFD, USA). The syringe was closed off by a pressure cap, placed onto a syringe holder, and manually primed to avoid any dead volume. The materials were extruded through the nozzle using a texture analyzer (Instron 5564, Norwood USA) with a load cell of 2000 N. A camera (UI–3160CP-M, Imaging Development System, Germany) with a zoom length lens (6.5X Zoom Lens, Edmund Optics, UK) was placed 5 cm from the nozzle to monitor the material surface just below the nozzle, during extrusion.

2.3. Development of CV-based calibration tool

A CV-based method is developed to determine instant extrusion rate and filament width during the extrusion of food materials. During the method development process, a texture analyzer was used to perform compression tests to mimic the actual printing process.

2.3.1. Extrusion force and video acquisition

The material (see section 2.1) was extruded from the syringe using a texture analyzer. The stainless-steel probe installed on the texture analyzer performed a uniaxial compression test with a displacement of 5 mm at rates between 5 and 15 mm/min. These rates of compression simulate the linear feed rates commonly used in 3D food printing. A double compression test was conducted to determine the compression force profile during extrusion for each printing material. A 30-s rest time was set in between two compressions to simulate the re-pressurizing step in a 3D printing syringe. Using the feed rate of the piston, the average extrusion rate of the material was estimated based on the continuity equation (Moretti et al., 2021).

$$V_{ex} = V_{feed}\left(\frac{D_2}{D_1}\right)^2 \quad (1)$$

where V_{nozzle} is the average extrusion rate (mm/s), V_{feed} is the displacement rate of the compression piston (mm/s), D_1 is the nozzle diameter (mm), and D_2 is the syringe diameter (mm).

For each double compression test, a camera with a fixed focal length lens (25 mm, Edmund Optics, UK) was placed 10 cm from the nozzle to monitor the extrusion process. The camera was controlled by the uEye Cockpit software (Imaging Development System, Germany). In the operating mode, the camera captures 300 × 400 pixel frames at frequencies ranged between 600 and 700 frames per second (FPS). The camera was triggered simultaneously with the compression to conduct synchronized measurements of extrusion rate and force. The corresponding compressive force and material extrusion video were recorded to characterize the extrusion process.

2.3.2. Extrusion rate measurement

Prior to the extrusion rate measurement, a scaling factor (F_s) was calculated to convert the pixel distance to the real distance using the outer diameter of the nozzle as a reference distance. The extrusion rate was measured by estimating the material movement between 2 consecutive frames. A pixel at position (x, y) was selected on the current frame to mark the original position of the printing material. In the next frame, the new position of this pixel, (x', y'), was estimated using the Lucas-Kanade optical flow algorithm (Lucas and Kanade, 1981). The algorithm works with three key assumptions: the pixels have not displaced significantly across consecutive frames, the neighboring pixels have the same displacement, and the pixel intensity changes are smooth across frames. These assumptions are valid for non-transparent printing materials that yield sufficient surface roughness to have resolution between pixels. The extrusion rate (v) between consecutive frames was calculated by dividing the distance travelled by the pixel in these frames by time per frame and scaling the result by F_s (equation (2)).

$$v = \frac{\sqrt{(x-x')^2 + (y-y')^2}}{t} \times F_s \quad \text{where} \quad t = \frac{1}{FPS} \quad (2)$$

The extrusion rate calculation between 2 frames was repeated until the point travelled 1 mm from the original point position. A new point was then selected back to the original position, and the same tracking process was repeated to ensure that the extrusion rate measured was within 1 mm below the nozzle (Fig. 1A and B). The 1 mm maximal

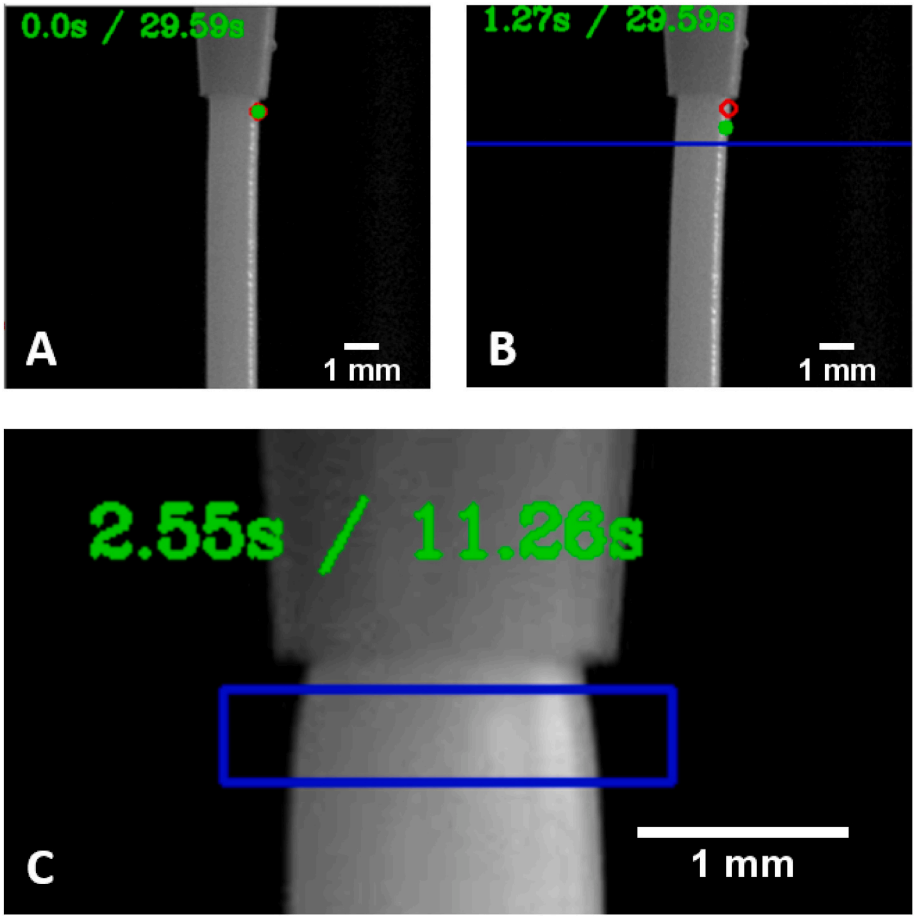

Fig. 1. A: a snapshot of the initial frame of an extrusion video. B: a snapshot of the tracking during extrusion. The red circle represents the original position of the material green dot represents the current position of the material, the blue line represents the 1-mm mark line. C: Extruded filament width measurement. The width of the extruded filament was measured within the blue bounding box (<1 mm below the nozzle).

distance minimizes the effect of gravity on the extrusion rate and was selected to represent a real 3D food printing situation in which the printing material is dispensed onto the platform or a previous layer within the distance equal to the nozzle diameter (ranged from 0.84 to 1.54 mm). The raw data was smoothened using the Savitzky–Golay filter with 31 neighboring points, making the final measurement frequency around 0.05 s/measurement. The smoothened extrusion rate was analyzed and compared to the average extrusion rate calculated from the feed rate of the piston using the continuity equation (eq. (1)). To evaluate the repeatability of the extrusion rate measurement, four different positions were tracked from the same video recording. The coefficient of variation (standard deviation divided by mean) of four measurements was calculated to understand the reliability of the CV-based measurement.

2.3.3. Extruded filament width determination

From the same extrusion video, the width of the extruded filament was measured to quantify the "die-swell" of food materials. A bounding box was put within 1 mm of the nozzle position to select the area of interest for the extruded filament width (Fig. 1C). The Canny edge detector was applied to determine the edge of the extruded filament (Canny, 1986). The row-wise pixel distance of the extruded filament was measured and converted into real distance using the calibration factor obtained from the extrusion velocity measurement (section 2.4). The extruded filament width was averaged per frame and recorded to characterize the extruded filament width change over time during food printing. The mode of the extruded filament width (D_{ex}, mm) was used for calculating the die swell ratio with the following equation (3):

$$Swell\ Ratio = (D_{ex} - D_n)/D_n \tag{3}$$

where D_n (mm) is the diameter of the extrusion nozzle.

2.4. Feedforward control of nozzle motion

The aforementioned CV-based calibration tool was applied in the actual printing of food material. Printing experiments were carried out using an extrusion-based 3D printer modified with a pneumatic 3D printing system equipped with a syringe heater (DR-2203, Nordson EFD, USA) (Schutyser et al., 2018). The motion control of the dispensing system is independent from the air-pressured extruder, allowing motion flexibilities such as acceleration and deceleration without impacting the extrusion flow.

2.4.1. Extrusion latency compensation

To compensate for the extrusion latency from the printer and the material elasticity, a nozzle motion acceleration profile was developed based on the measured extrusion rate. The printing materials were carefully loaded into a printing syringe, and the syringe was closed off with a pressure cap and tempered at printing temperatures between 20 and 50 °C for 10 min prior to printing. The same camera (see section 2.2) was placed 10 cm from the printing nozzle to capture a point dispensing of the printing material. The extrusion rate (V_{ex}) of the material was measured using the CV-based method introduced in section 2.4. The nozzle velocity (V_n) profiles were calculated with the continuity equation (eq. (4)).

$$V_n = V_{ex}\left(\frac{D_{ex}}{D_t}\right)^2 \tag{4}$$

where D_{ex} (mm) represents the width of the extruded filament, and D_t (mm) represents the target extrusion width. For extrusion latency compensation experiments, the D_{ex} and D_t were set to be equal to each other, assuming no die swell during extrusion.

Five parallel lines of 80 mm were printed using constant and calibrated nozzle motions. This printing pattern was chosen to showcase the re-pressurizing process of the syringe (i.e. start-stop cycles) before printing a next line when under-extrusion of viscoelastic materials often occurs (Fahmy et al., 2020a; Nijdam et al., 2021). The length accuracy of the lines was expressed as a percentage of the actual length measured using ImageJ software divide by the target length times 100.

2.4.2. Customized extrusion line width

By controlling the nozzle velocity, one can minimize the effect of the die swell and customize the extrusion line width. Based on eq. (4), the target extrusion width (D_t) is usually set to be the width of the nozzle (although one can alter the extrusion line width based on different nozzle motion profiles (Moetazedian et al., 2020)). To demonstrate the extrusion line width customizations, squares with 3 different target widths were printed for white chocolate spread, cookie dough, and processed cheese. Using the ImageJ software, the actual printed width was measured from duplicated printings. The accuracy of the extrusion width customization was expressed as a percentage of the measured width divide by the target width times 100.

2.5. Software development and availability

The CV software was developed in-house using the OpenCV, NumPy, Pandas, and PIMS libraries in the Python programming language. The software, including a graphical user interface, raw scripts, and demonstrations can be accessed through https://git.wur.nl/yizhou.ma/extrusion-flow-tracker.

3. Results and discussions

3.1. Printing material characterizations

Four representative food materials used for printing were selected, differing in their rheological behavior, printing temperatures (20 °C or 50 °C) and surface roughness. The rheological behavior influences the extrusion and the appearance influences the optical measurement of extrusion rates (Greeff and Schilling, 2017; Liu et al., 2019a, 2019b). Fig. 2 shows the frequency sweeps of the printing materials. The storage and elastic moduli of all four materials showed power-law dependencies on the shear frequency, indicating that the materials are viscoelastic soft solids that are suitable for 3D food printing applications (Sridharan et al., 2021). The storage moduli of cookie dough, lemon curd, and white chocolate spread are greater than the loss moduli at all frequencies measured, indicating a solid-like rheological behavior for these three materials, which allows extrusion at room temperature. White chocolate spread has the highest storage modulus, showing more elasticity than cookie dough and lemon curd. Although the printing materials differ in terms of storage and loss moduli, the solid-like materials fall into the typical range of storage moduli as reported by other 3D food printing studies (Liu et al., 2020a, 2020b; Zhu et al., 2019). Processed cheese has a melting transition at the measuring temperature of 50 °C, and therefore at frequencies below 15 rad/s, behaves liquid-like. This liquid-like behavior is required for extrusion and fusion of the printed cheese (Le Tohic et al., 2018). This melting transition gave the processed cheese more frequency-dependency compared to the other food materials and stronger shear-thinning behavior. The rheological properties of the four printing materials are consistent with those reported in previous literature, which illustrates their suitability to use as representative materials for examining the feedforward control method developed in this study.

In addition to rheological properties, surface opacity and surface roughness of the food materials are important as they may influence the performance of the optical flow tracking algorithm (Greeff and Schilling, 2017). Optical methods are in general limited to opaque materials with rough surfaces because the optical flow algorithm tracks changes in pixel intensity during extrusion (Nuchitprasitchai et al., 2017). Fig. 3 shows the surface roughness of the 4 printing materials as they were extruded out of the nozzle. Inhomogeneity in the materials caused

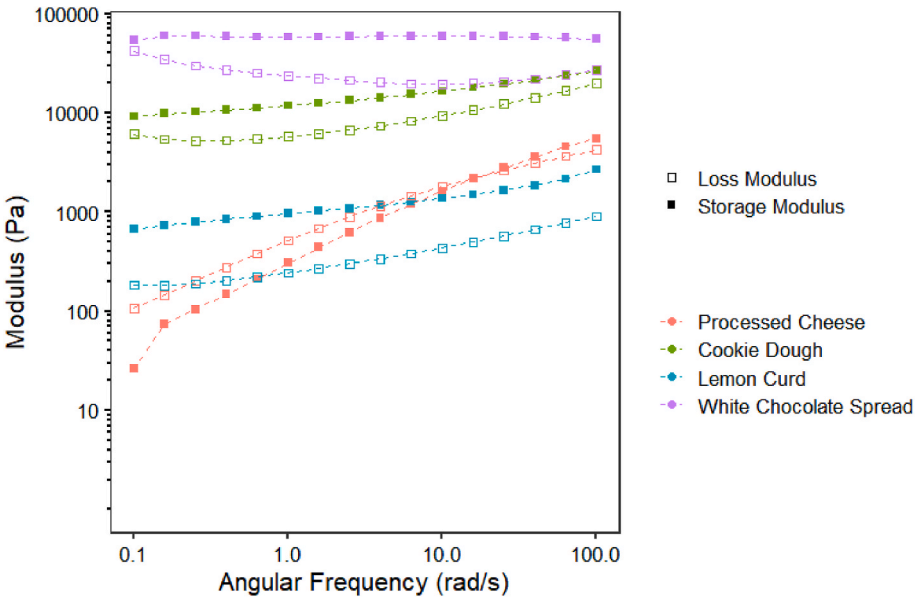

Fig. 2. Frequency sweeps of white chocolate spread, lemon curd, cookie dough, and processed cheese. White chocolate spread, lemon curd, and cookie dough were measured at 20 °C, and processed cheese was measured at 50 °C. The closed symbols represent the storage modulus, and the open symbols represent the loss modulus obtained under a constant shear strain of 0.5%.

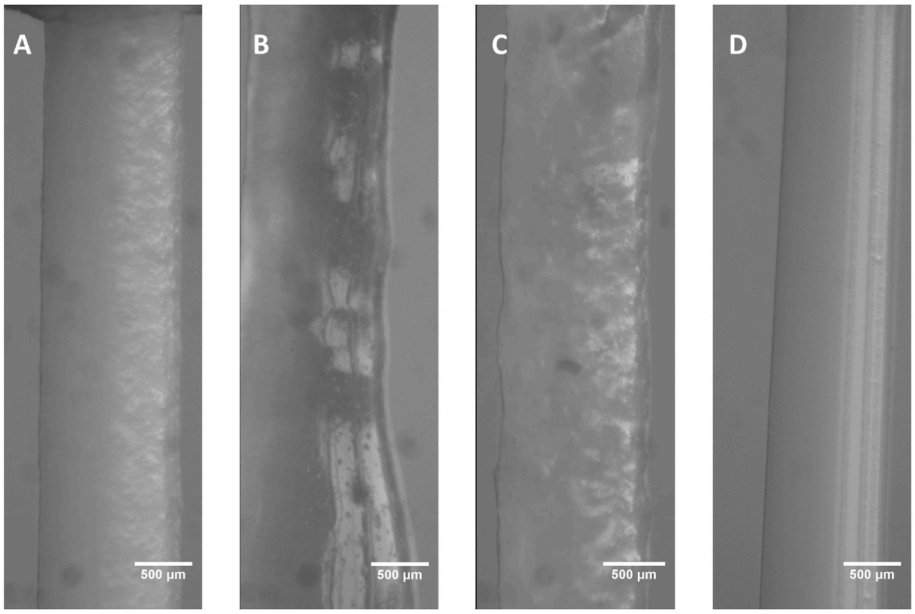

Fig. 3. Surface roughness of the printing materials. A: white chocolate spread, B: lemon curd, C: cookie dough, and D: processed cheese. Samples were imaged as they were extruded from the printer using a 6.5 X zoom length lens.

somewhat irregular extrusion rates which then resulted in grains and cavities on the surface of all 4 materials, providing sufficient surface roughness for optical motion tracking. Preliminary experiments with smooth-surface hydrogels made from sodium alginate (i.e. a common bioprinting material) showed these to be unsuitable for optical tracking methods. Therefore, the method proposed in this study is aimed at opaque materials with some degree of surface roughness, as food materials commonly are.

3.2. Extrusion rate measurement

The precision of the CV-based method for extrusion rate measurement was first evaluated. White chocolate spread was extruded using a double compression that was described in section 2.4 at 20 mm/s feed rate, and the corresponding material extrusion was recorded and analyzed. Using the same video recording, the extruded filament tracking was repeated 4 times and the corresponding extrusion rate was calculated. From the 4 repeated extrusion rate measurements shown in Fig. 4A, a coefficient of variation of 1.19% was derived. This small variation showed that the CV-based measurement is repeatable, indicating its reliability as a calibration tool for 3D food printing.

The measurement accuracy was also examined by combining the extrusion force measurement and the average extrusion rates calculated from the continuity equation (eq. (1)). Fig. 5A shows the extrusion force profiles of printing the white chocolate spread. At the initiation stage of the extrusion, a latency period was observed as the force gradually

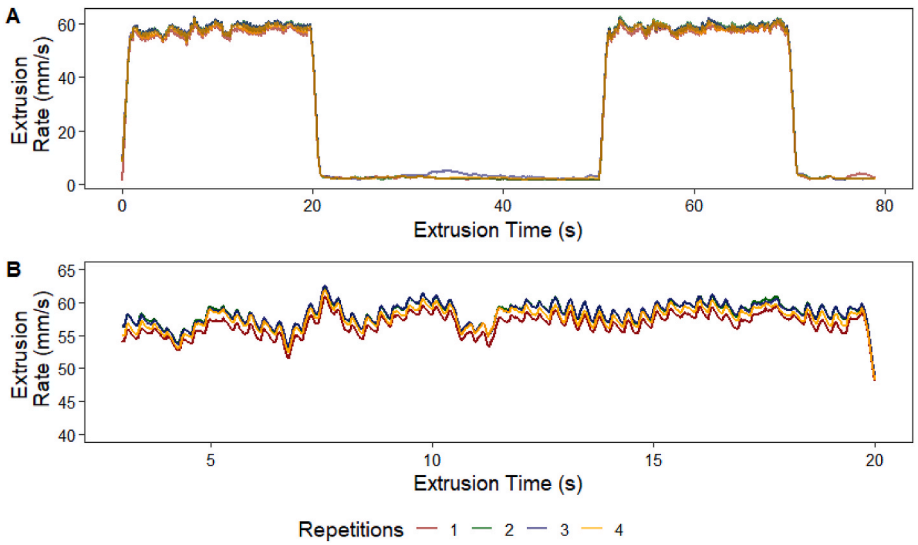

Fig. 4. A: Four repeated analysis of the same video recording of white chocolate spread during extrusion, using the developed CV-based method. B: zoomed in stable range of the extrusion rate; the coefficient of variation in the stable extrusion range is 1.19%.

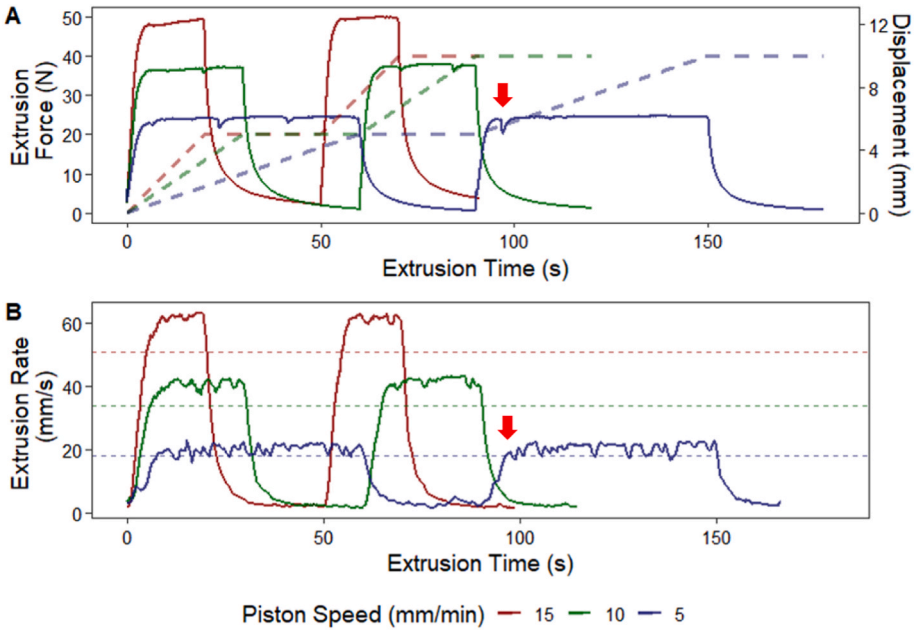

Fig. 5. Results obtained from the double compression test of white chocolate spread at different piston displacement speed of 5, 10, and 15 mm/min. A: extrusion force (solid lines, primary y-axis) and accumulated displacement distance of the piston (dashed lines, secondary y-axis) over time. B: extrusion rate over time; the dotted line in B represents the average extrusion rate calculated from the continuity equation (eq. (1)). The red arrows point at drops of extrusion force and rate, which was likely caused by the inhomogeneity of the sample.

increased while the piston displacement moved at a constant rate. The latency was caused by compressibility of the syringe holder and food materials. Even though pure food materials are often incompressible, in complex food systems, small air bubbles can often be suspended in food materials, contributing to the apparent compressibility from the printed foods. As a result, in real printing applications, the latency is often linked to the under-extrusion at the beginning of printing a structure. As the compression continued, the measured force plateaued until the end of the pressing cycle. When the piston movement stopped, the extrusion force gradually decreased until the second compression started, while the remaining pressure in the syringe continues to push materials out of the nozzle. The graduate release of syringe backpressure often corresponds to the over-extrusion (i.e. oozing) of material during printing.

A similar force increase and a plateau were observed for the second compression period. The extrusion force profiles were consistent across different piston feed rates, and a faster feed rate always resulted in shorter time taken to reach the force equilibrium. Such changes in force were also observed from the extrusion rate measurements as shown in Fig. 5B. Due to the changes in the extrusion force, the extrusion rate also accelerated and decelerated again during the extrusion (i.e. in each start-stop cycle). The acceleration of the extrusion rate lasts between 2 and 5 s depending on the different feed rates. Prior to the plateau phase, the extrusion latency leads to under-extrusion issues if the nozzle motion is set constant. Therefore, incorporating of an acceleration phase in nozzle motion (i.e. a calibration) can compensate for the extrusion latency caused by syringe pressurization and food compressibility.

The extrusion force and rate profile of plastics were measured and reported in several other studies. Similar acceleration phases were reported before reaching the extrusion force equilibrium (Moretti et al., 2021; Serdeczny et al., 2020a). For plastic printing reported in literature, the extrusion force and rate changes are smoother than that were observed from food extrusions. This is likely due to the more homogeneity of these plastics, while the heterogeneity and air bubbles trapped in the food materials lead to some irregularity in the extrusion.

However, as shown in Fig. 5, a sudden decrease in force is often matched with a sudden decrease in extrusion rate, showing that the extrusion rate measurement is fully consistent with the force measurement. The dashed lines in Fig. 5B show the average extrusion rate calculated from the continuity equation (eq. (1)). These average rates underestimate the actual extrusion rate because the continuity equation ignores the extrusion acceleration at the beginning of each push. This underestimation is proportional to the extrusion rate: a larger underestimation was observed for the faster extrusion rate. When the nozzle motion was referenced to this average extrusion rate (i.e. a constant nozzle movement speed is chosen throughout printing), it is likely that the extrusion will suffer from inconsistency due to acceleration and deceleration during actual extrusions.

Fig. 6 shows the results obtained from the double compression experiments conducted for lemon curd. The extrusion force and rate matched, similar to the white chocolate experiment. The jelly-type material required much less force to extrude because of its lower storage modulus compared to the white chocolate spread (Fig. 2). The lemon curd also showed more variation in the extrusion rate and force measurements, which is likely because of the air bubble trapped in the material. The inhomogeneity of the lemon curd was reported earlier by Vancauwenberghe et al. (2017) when printing pectin-based snack foods (Vancauwenberghe et al., 2017). The porosity and rough surface of the extruded filament confirmed that air bubbles can impact the final printing outcome of pectin-based foods (Fig. 3B). Such inhomogeneities in food materials are randomly distributed, which leads to challenges to establish predictive models to counter such effects. A feedforward approach can adapt to the general acceleration and deceleration phases appearing in the extrusion rate profile, but it is still incapable of reacting to the small, fast variations in extrusion rate caused by the inhomogeneity. As an alternative solution, pre-treatments such as centrifugation/degassing has been used by others to achieve consistent food texture before printing (Zhu et al., 2019). Overall, the CV-based extrusion rate measurement agrees well with the extrusion force measurement. The measured instant extrusion rates appeared to be dynamic and greater than the averaged extrusion rate, which provides the necessary information for the subsequent nozzle motion planning step in this study.

3.3. Extruded filament width measurement

While measuring the extrusion rate, the width of the extruded filaments was also measured to characterize the die swell during extrusion. Fig. 7 shows the change of the extruded filament width over time for processed cheese and white chocolate spread. The two materials vary largely in compositions, which is also reflected in their differences in die swell during extrusion. For white chocolate spread, a swelling ratio of ~0.15 is observed for extruded filaments printed at 1, 1.5, and 2 bars. The initial extruded filament width (ranged between 0.2 and 0.6 mm) expanded to a stable width of 0.95 mm in less than 0.5 s (Fig. 7A). The initial width expansion is likely to be caused by the velocity distribution during pipe flow as materials closer to the center of the pipe travel faster than closer to the wall (Haavisto et al., 2017). The swell of the extruded filament is relatively independent from the extrusion pressure range, suggesting that the increase of the extrusion pressure, therefore the wall shear stress, has negligible influence on the die swell. Sombatsompop and Dangtangee reported a logarithmic relation between the wall shear stress and the die swell of viscoelastic fluids (Sombatsompop and Dangtangee, 2002). They showed that above a certain threshold of wall shear stress, the die swell ratio becomes relatively independent of the wall shear stress. The white chocolate spread used in this study behaves similarly, with a consistent die swell ratio of 0.15 across different extrusion pressures.

For the extruded processed cheese filaments, more die swell (die swell ratio = 0.3) was observed compared to the white chocolate spread (Fig. 7). Processed cheese contains casein micelles which deform during flow and relax back towards their original shape upon pressure release. The processed cheese also showed an initial width expansion, most probably attributed to its unique rheological properties related to the deforming casein micelles. Note that the initial width of the processed cheese filament was higher than that of the white chocolate spread, likely because processed cheese is more shear-thinning as shown in Fig. 2 (i.e. the moduli of processed cheese is more impacted by the increase of shear frequency). The higher degree of shear-thinning leads to a 'flatter' velocity profile in the pipe resulting in flow closer to plug flow, which ultimately leads to the wider initial extruded filament width observed here (Haavisto et al., 2017). Uniquely observed for processed

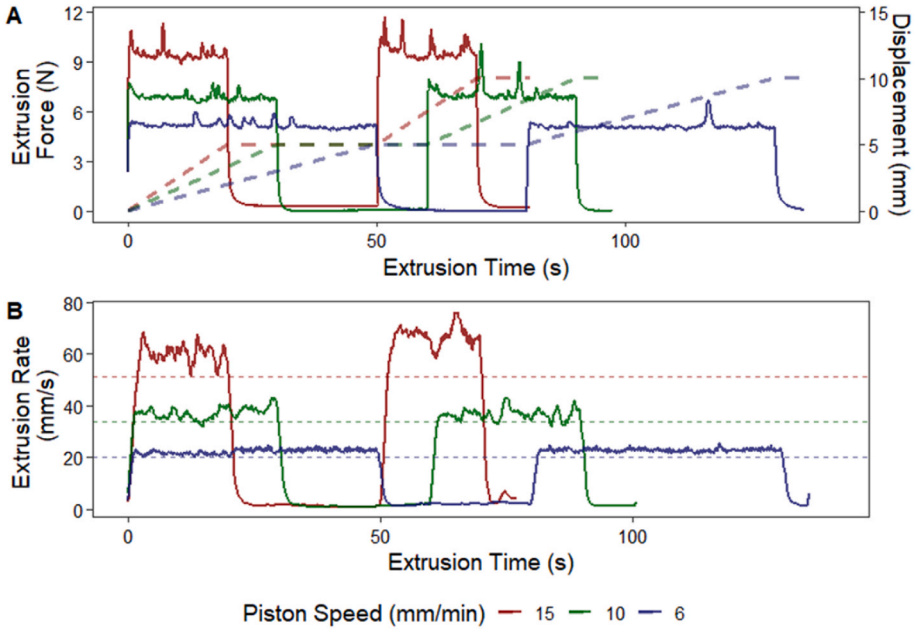

Fig. 6. Results obtained from the double compression test of lemon curd at different piston displacement speed of 6, 10, and 15 mm/min. A: extrusion force (solid lines, primary y-axis) and accumulated displacement distance of the piston (dashed lines, secondary y-axis) over time. B: extrusion rate over time; the dotted line in B represents the average extrusion rate calculated from the continuity equation (eq. (1)).

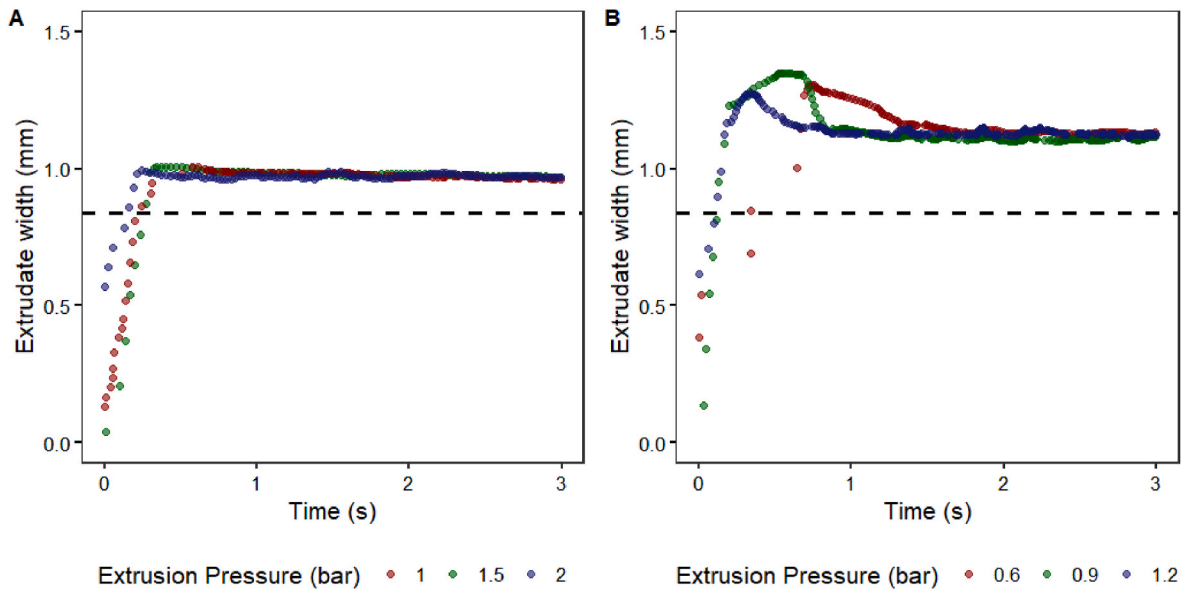

Fig. 7. Extruded filament width measurement over time. A: white chocolate spread. B: processed cheese. The black dashed line represents the inner diameter of the printing nozzle (0.84 mm).

cheese, the die swell was initially very fast, which then slowed down and attained a stable width. The large initial width expansion can be attributed to the cooling of the material at the nozzle: preliminary experiments suggested a 10 °C temperature drop between the set extrusion temperature and the actual nozzle temperature. This temperature drop lead to increased elasticity during flow, which created more back-pressure during extrusion and a higher initial swell of the material. After the initial swell, the melted cheese was continuously extruded to reach a steady state of a consistent width expansion. During the steady state, a minimal impact of extrusion pressure was found on extruded filament width, suggesting that the applied extrusion pressure range (0.6–1.2 bar) had small impact on die swell. Overall, both processed cheese and white chocolate spread swell upon extrusion, indicating that the extruded filament width is greater than the nozzle size (Ma et al., 2021; Ross et al., 2021). The measured extruded filament width can be used as inputs to dynamically control the printed filament width by customizing the printing speeds.

3.4. Feedforward control of nozzle motion

3.4.1. Extrusion latency compensation

Several food materials were printed using a pneumatic 3D printer to implement the feedforward control of nozzle acceleration. For all materials, the printing pressure was adjusted to achieve extrusion rates of ~40 mm/s to simulate regular food printing. The CV-based method was used to determine the onset of extrusion, and the measured extrusion rates were used to find the required nozzle acceleration for feed forward control. Fig. 8 shows the nozzle acceleration and the corresponding lines printed using white chocolate spread, cookie dough, and processed cheese. The nozzle velocity (~40 mm/s) was set to match the plateau velocity that would lead to the required steady-state line width based on the extrusion rate measurement. The printed lines with a constant nozzle motion suffered from under-extrusion as they appeared to be shorter than those printed with a calibrated nozzle motion (Fig. 8). The accuracies of the printed lines are summarized in Table 1. For the three printing materials, the calibrated printing achieved accuracies ranged from 97.9 to 100%. Compared to the constant printing, the calibrated printing improved the length accuracies ranging from 4.7 to 10.6%. The under-extrusion was consistently found to be at the beginning of the line extrusion, which corresponds to the start-stop point of 3D printing. As the printing syringe is pressurizing, the under-extrusion is likely caused by the high elasticity and yield stress of the food materials (Fahmy et al., 2020b). Under air pressure, the food materials, which may contain some air bubbles, can be compressed somewhat before extrusion, leading to latency and a slower acceleration in extrusion. Fig. 8 also shows that each material has a unique acceleration profile, which is related to their rheological properties – other studies showed that shear thinning influences the extrudability of food materials (Liu et al., 2019a, 2019b; Ma et al., 2021). Preliminary measurements suggested that the white chocolate spread was the most shear-thinning sample compared to the cookie dough and processed cheese. The white chocolate spread also required the least amount of distance to reach the 40 mm/s steady speed. The flow rate of shear-thinning materials follows a power-law relation as a function of pressure, suggesting that white chocolate spread is more sensitive to pressure change, which resulted in a faster acceleration than the other less-shear-thinning materials.

In Fig. 8C and Table 1, processed cheese shows the most severe under-extrusion and the least accurate length under constant printing. From the rheological measurements (Fig. 2), melted processed cheese (50 °C) has moderate elasticity and is liquid-like at low frequency (below 15 rad/s). The under-extrusion of processed cheese was likely caused by the change in nozzle temperature during printing. The temperature drop caused a solidification of the cheese, which lead to delayed extrusion and subsequent larger 'blob' of deposited cheese, as shown in Fig. 8C. Extrusion accuracy improved for the last 2 lines printed in Fig. 8C, suggesting that the previously printed lines may have warmed the nozzle such that subsequent lines were more accurately printed. The improved printing length may also contributed to the larger length accuracy standard variation found for the processed cheese (Table 1). This nozzle temperature effect of cheese was also observed from the extruded filament width measurement (Fig. 7B), as an initial swell was observed, which corresponds to the "rounded tip" on the constantly printed lines. The delayed extrusion was also captured by the CV-based method, and the feedforward nozzle acceleration prevented under-extrusion. Such an extrusion latency can be alleviated by a nozzle heater to better control the extrusion temperature at the nozzle. Despite different reasons that can cause under-extrusion, the CV-based method was able to measure the extrusion rate, implement the feedforward control, and improve the printing accuracy.

3.4.2. Customized extrusion line width

After compensating for the extrusion latency, extrusion line width

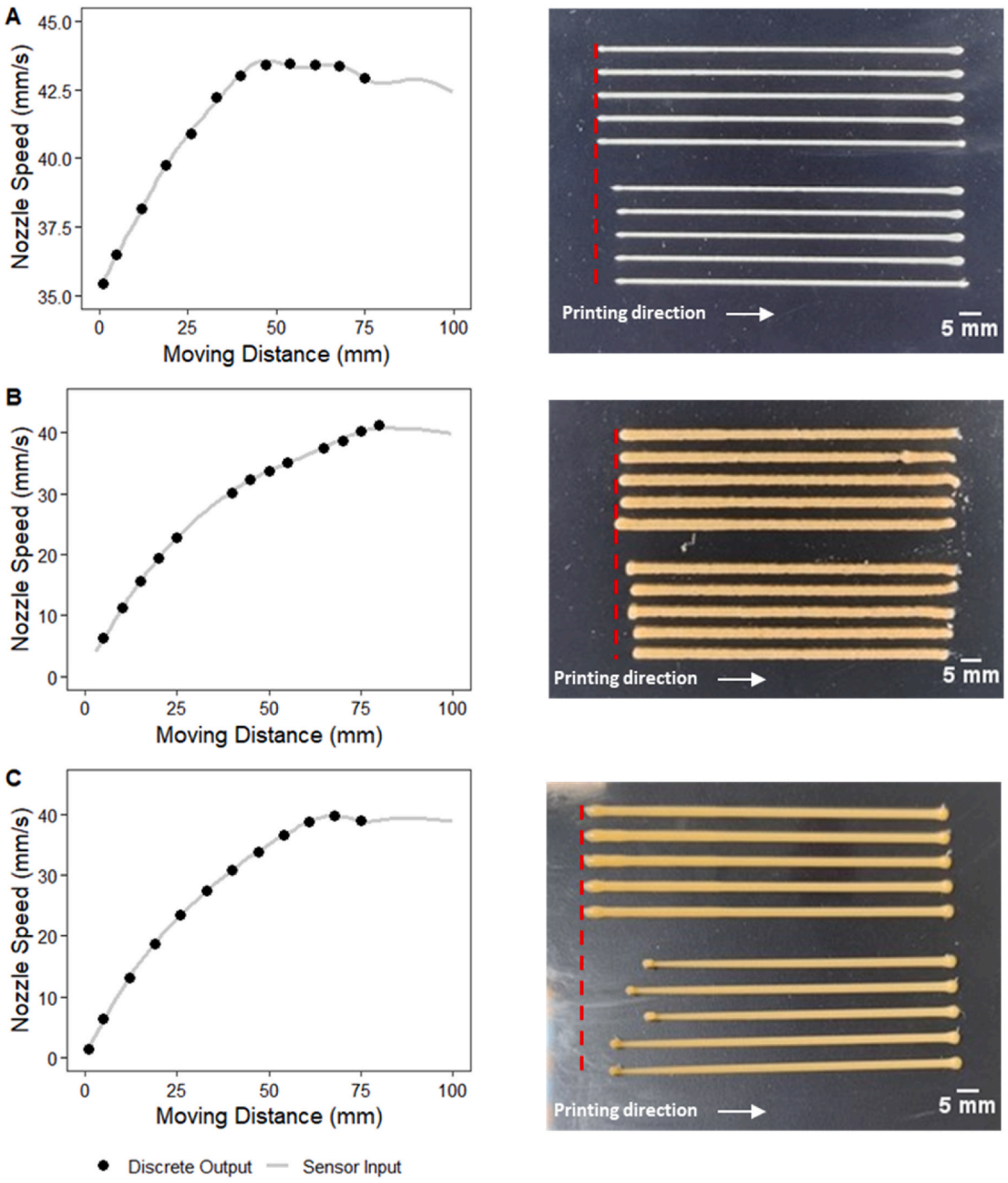

Fig. 8. Calibrated nozzle motion profiles and printing results. A: white chocolate spread, B: cookie dough, C: processed cheese. The top 4 stripes were printed with calibrated nozzle motion and the bottom 4 stripes were printed with constant nozzle motion. The round dots represent the discrete outputs sent to the printer to achieve the calibrated printing. The red dashed lines represent the start position of the line extrusions.

customization was further implemented. Based on the extruded filament width measurement, nozzle velocity was adjusted based on the intended filament width (eq. (4)). Fig. 9 shows the nozzle velocity profiles needed to achieve the target printing width for the printing materials. The nozzle velocity profiles in Fig. 9A, C, and E are similar to those shown in Fig. 8. The initial accelerations compensated the extrusion latency, and the slope and peak nozzle velocity determined the width of the extrusion lines. As reported in other studies, altering the nozzle motion can result in differences in extrusion line width (Comminal et al., 2019; He et al., 2016; Ma et al., 2021). The examples shown in this study suggest that one can better achieve the target extrusion width by controlling the nozzle velocity based on the continuity of volume transfer, when the extrusion force/pressure was kept constant. To assess the width customization accuracies, Table 2 provides the width printing accuracies compared to the target widths. The measured line widths validate the control strategy because the width accuracy ranged between 95 and 107% (above 100% means over-extrusion). Width variations were represented by the standard deviation of the width accuracy. By visual inspections in Fig. 9B, D, and F, the targeted line width was achieved on most positions of the square, except at corners. Over-extrusion was found on the corners due to the deacceleration of the nozzle when making turns. The degree of over-extrusion increases with faster

Table 1
Printing length accuracy comparison between calibrated and constant printing of white chocolate spread, cookie dough, and processed cheese. (Target line length = 80 mm).

Printing Profile	Sample	Length accuracy ± standard deviations (%)
Calibrated	White Chocolate Spread	99.0 ± 0.6
	Cookie Dough	97.9 ± 1.1
	Processed cheese	100.0 ± 1.2
Constant	White Chocolate Spread	93.7 ± 0.7
	Cookie Dough	93.2 ± 1.7
	Processed cheese	89.4 ± 5.2

printing velocity, and this is due to the stronger deceleration needed for faster printing. This mechanical limitation of the printing platform can lead to printing inaccuracies, as also reported by Comminal et al. (2019). The width customization developed in this study can be potentially implemented to better printing complex structures when different printing resolutions are needed, by dynamically controlling the printing motion.

3.4.3. *Printing improvement demonstration*

To further illustrate the improvement in printing that can be achieved with the CV-based method, Fig. 10 shows a top-view comparison of a single layer and a sideview comparison of layer stackings. The graphic design in Fig. 10A was printed by four continuous lines. The red arrows point at the pressuring/starting position of a new extruded line. Similar to the observations in Fig. 8, with a constant nozzle motion, under-extrusion was observed at the start of each extrusion, resulting in gaps in the single layer extrusion. With the nozzle acceleration implemented, the under-extrusion was much reduced to improve the layer completion (Fig. 10B). The under-extrusion of each layer can also harm layer stacking and cause slippage (Fig. 10C). With the calibrated nozzle

Table 2
Accuracy evaluation of the customized extrusion width of white chocolate spread, processed cheese, and cookie dough.

Sample	Target width (mm)	Width accuracy ± standard deviations (%)
White Chocolate Spread	0.8	104.9 ± 5.0
	1.0	107.0 ± 5.4
	1.5	101.7 ± 2.7
Processed cheese	1.2	100.4 ± 2.9
	1.5	95.0 ± 7.4
	2.0	100.8 ± 4.9
Cookie Dough	1.8	105.0 ± 3.8
	2.5	95.8 ± 2.0
	3.0	101.0 ± 4.3

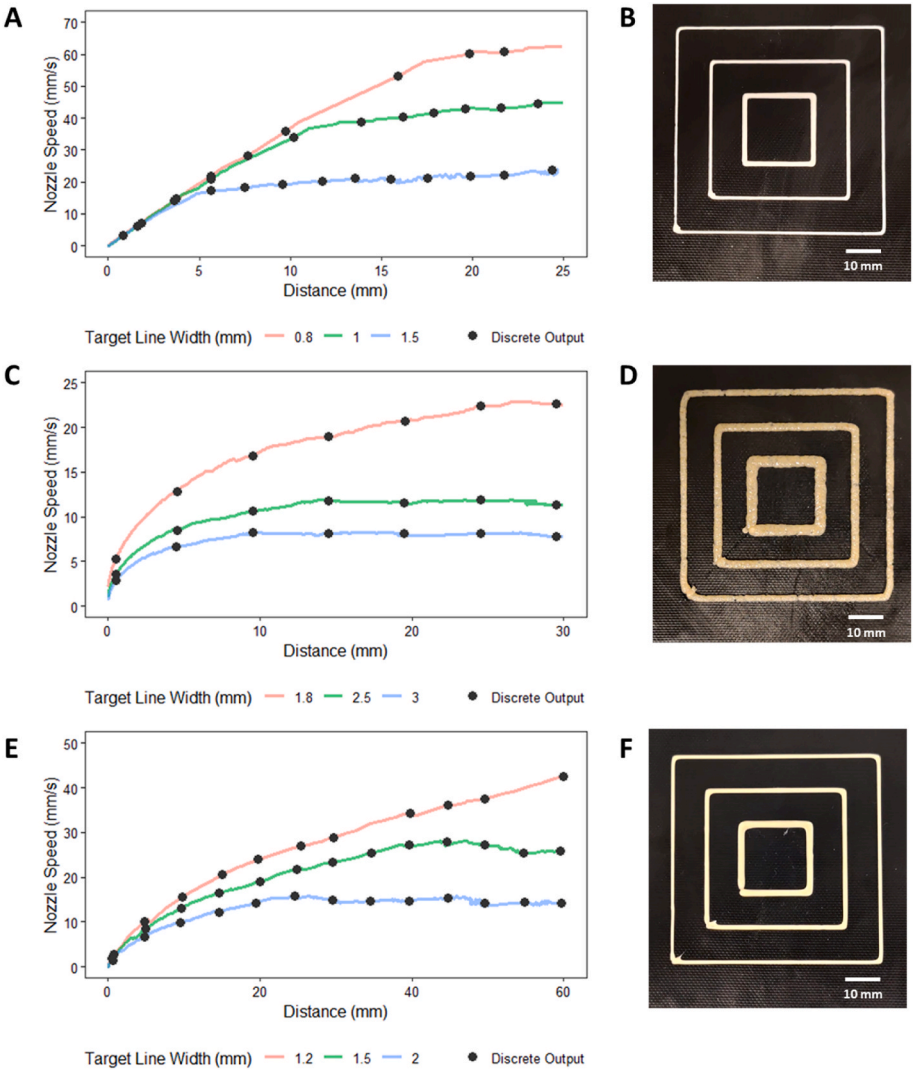

Fig. 9. Customized extrusion line width showcase. A: nozzle (⌀ 0.8 mm) velocity profiles for white chocolate spread of different target line widths. B: Printed squares based on customized extrusion line width. Outer square (0.8 mm), middle square (1.2 mm), and inner square (1.5 mm). C: nozzle (⌀ 1.8 mm) velocity profiles for cookie dough of different target line widths. D: Printed squares based on customized extrusion line width. Outer square (1.8 mm), middle square (2.5 mm), and inner square (3 mm). E: nozzle (⌀ 1.2 mm) velocity profiles for processed cheese of different target line widths. F: Printed squares based on customized extrusion line width. Outer square (1.2 mm), middle square (1.5 mm), and inner square (2 mm).

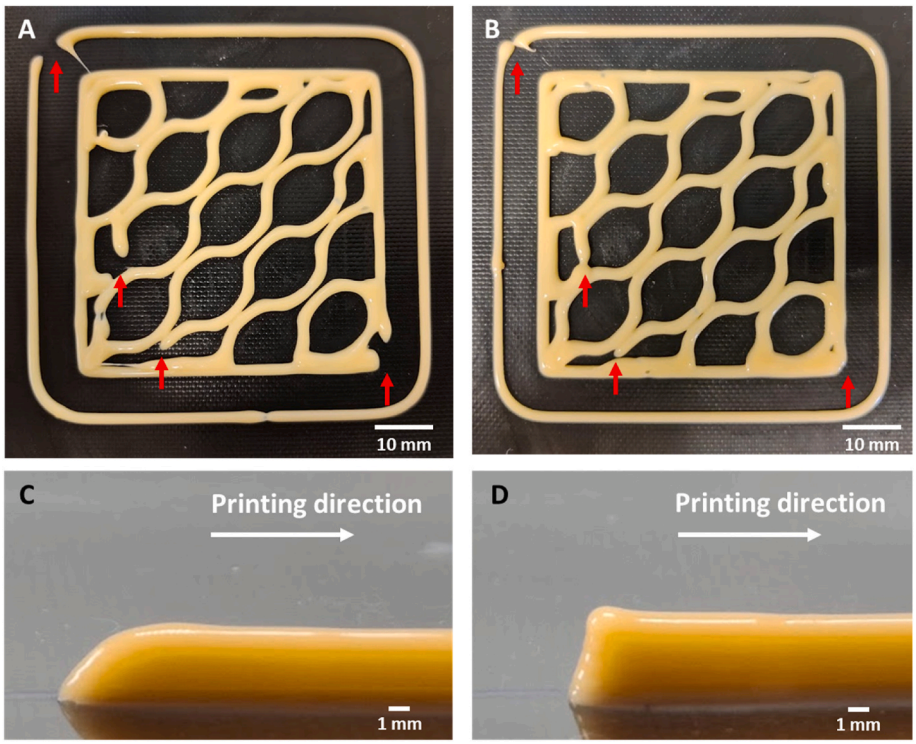

Fig. 10. Printing accuracy improvement showcase. A: a processed cheese honeycomb layer printed with constant nozzle motion. B: a processed cheese honeycomb layer printed with calibrated nozzle motion. C: Sideview of layered processed cheese printed with constant nozzle motion. D: Sideview of layered processed cheese printed with calibrated nozzle motion. The red arrows in A and B indicate the pressurizing positions of the printing path.

motion, each layer was better extruded and stacked to achieve accurate printed structures (Fig. 10D).

3.5. General discussion

While the CV-based feedforward control method can give practical and good printing accuracy improvement, it still carries a few limitations. First, the printing materials should be sufficiently opaque and have sufficient surface roughness to create pixel intensity differences that can be picked up by the algorithm. Without pixel intensity changes among the frames, it is impossible to track the extruded filament movement and measure the extrusion rate based on an optical method. Second, the feedforward control of the nozzle motion assumes that the robotic platform can achieve sufficient acceleration to ensure an almost-constant instant nozzle velocity. Too large variation of the nozzle velocity during printing will result in over-extrusion, due to insufficient acceleration and deceleration (as observed in Fig. 9), and one should reduce the nozzle plateau velocity to better match the printer's capacity (Ertay et al., 2018). In this study, a pneumatic dispensing system was used to independently control nozzle motion and extrusion, which realized the printing accuracy improvement. However, the traditional G-code-based control treats the extrusion axis as a secondary axis to the motion, which limits the motion control independency demonstrated in this study. Lastly, since the calibration step relies on data obtained from a static extrusion, gravity effects were ignored when calculating extrusion rate and extruded filament width. When applying this method in practice, extrusion rate tracking and extruded filament width measurement should focus only on 1 mm below the nozzle, to minimize gravitational impacts.

With the assumptions in mind, the feedforward control method uses a CV-based calibration step to determine the nozzle motion for printing food materials. Compared to other flow rate measurements such as ultrasound and conductivity, the CV-based method is simple and modular, and easy to re-implement on existing 3D food printers. The open-source video analysis software, that is made publicly available with this study, includes a user-friendly graphical interface to conduct the required measurements. The feedforward control that is discussed in this study does not provide feedback for in-process control (although it could be combined with this in principle, and is a potential future application). However, because of the varying material properties of food, the simplicity and flexibility of this CV-based method makes its implementation for 3D food printing applications straightforward, avoiding time and resources expenditure in trial-and-error experiments, as is usually required. With this method, 3D food printing will further advance as an on-demand tool that can rapidly and accurately manufacture foods based on consumer needs, without requiring much more complicated equipment and increasing food production efficiency.

4. Conclusions

This study developed and evaluated feedforward control of the nozzle motion to optimize the extrusion line width and improve the printing accuracy. A sideview camera filmed the extrusion of food materials at the nozzle to in-situ measure the extrusion rate and extruded filament width using an optical flow algorithm. This CV-based method is repeatable and reliable and works with opaque materials with surface inhomogeneity (as is the case for most food printing materials). The initial extrusion latency caused by the elasticity of the food materials, was compensated in the nozzle motion which led to much better initial extrusion line consistency. The extruded filament width measurement was used to customize filament width to achieve a higher degree of flexibility in 3D food printing. Three food printing materials were tested using the feedforward control to characterize material variations, and the method prevented under-extrusion of the food materials and improved printing accuracy in terms of 2D layer formation and 3D filament stacking. This CV-based method is simple to be implemented on most extrusion-based food printers as a material calibration tool to improve printing accuracy and avoid extensive trial-and-error

experiments in 3D food printing. Future research can focus on implementing the CV-based method in close-loop controls of 3D food printing to automate the parameter optimization process.

Author statement

Yizhou Ma: Conceptualization, Methodology, Investigation, Data analysis, Writing of the original manuscript. Jelle Potappel: Methodology, Investigation, Data analysis. Aneesh Chauhan: Conceptualization, Editing of the manuscript. Maarten A.I. Schutyser: Conceptualization, Supervision, Editing of the manuscript. Remko M. Boom: Supervision, Editing of the manuscript. Lu Zhang: Conceptualization, Supervision, Writing, review & editing of the manuscript.

Declaration of competing interest

The authors declare to have no conflicting interests.

Data availability

Data will be made available on request.

Acknowledgments

The authors would like to acknowledge the financial support from Sectorplan Techniek Mechanical Engineering (NWO).

Appendix A. Ingredient lists and purchase dates of commercial food products used in this study

Product	Purchase Date	Ingredients
ERU Slices Cheddar	March 2021	55% cheese (of which 50% cheddar), water, milk proteins, whey powder, butter, melting salts (e452), salt, coloring (paprika extract).
AH Chocoladepasta wit	March 2021	Sugar, vegetable oil (rapeseed, palm), dried skimmed milk powder, vegetarian whey powder, cocoa butter, whole milk, milk fat powder, emulsifier (lecithin [E322]), vanilla aroma, antioxidant (tocopherol-rich extract [E306]).
Chivers Lemon curd	March 2021	Sugar, water, palm oil, lemon juice from concentrate (3%) maize flour, egg powder, food acids (citric acid, acetic acid), gelling agent (pectin), acidity regulator (sodium citrate), lemon oil (0.16%), color (carotenes), antioxidant (ascorbic acid).
Dawn Cookie Mix Plain	May 2021	Wheat flour, sugar, vegetable oil, demerara sugar, whole egg powder, whey solids, dextrose, raising agent (sodium bicarbonate), glucose syrup, salt, natural flavoring.

References

Canny, J., 1986. A computational approach to edge detection. In: IEEE Transactions on Pattern Analysis and Machine Intelligence PAMI-8, pp. 679–698. https://doi.org/10.1109/TPAMI.1986.4767851.

Comminal, R., Serdeczny, M.P., Pedersen, D.B., Spangenberg, J., 2019. Motion planning and numerical simulation of material deposition at corners in extrusion additive manufacturing. Addit. Manuf. 29, 100753 https://doi.org/10.1016/j.addma.2019.06.005.

Derossi, A., Caporizzi, R., Paolillo, M., Oral, M.O., Severini, C., 2021. Drawing the scientific landscape of 3D Food Printing. Maps and interpretation of the global information in the first 13 years of detailed experiments, from 2007 to 2020. Innovat. Food Sci. Emerg. Technol. 70, 102689 https://doi.org/10.1016/j.ifset.2021.102689.

Ertay, D.S., Yuen, A., Altintas, Y., 2018. Synchronized material deposition rate control with path velocity on fused filament fabrication machines. Addit. Manuf. 19, 205–213. https://doi.org/10.1016/j.addma.2017.05.011.

Fahmy, A.R., Becker, T., Jekle, M., 2020a. 3D printing and additive manufacturing of cereal-based materials: quality analysis of starch-based systems using a camera-based morphological approach. Innovat. Food Sci. Emerg. Technol. 63, 102384 https://doi.org/10.1016/j.ifset.2020.102384.

Fahmy, A.R., Becker, T., Jekle, M., 2020b. 3D printing and additive manufacturing of cereal-based materials: quality analysis of starch-based systems using a camera-based morphological approach. Innovat. Food Sci. Emerg. Technol. 63, 102384 https://doi.org/10.1016/j.ifset.2020.102384.

Go, J., Schiffres, S.N., Stevens, A.G., Hart, A.J., 2017. Rate limits of additive manufacturing by fused filament fabrication and guidelines for high-throughput system design. Addit. Manuf. 16, 1–11. https://doi.org/10.1016/j.addma.2017.03.007.

Greeff, G.P., Schilling, M., 2017. Closed loop control of slippage during filament transport in molten material extrusion. Addit. Manuf. 14, 31–38. https://doi.org/10.1016/j.addma.2016.12.005.

Guo, C., Zhang, M., Devahastin, S., 2020. 3D extrusion-based printability evaluation of selected cereal grains by computational fluid dynamic simulation. J. Food Eng. 286, 110113 https://doi.org/10.1016/j.jfoodeng.2020.110113.

Haavisto, S., Cardona, M.J., Salmela, J., Powell, R.L., McCarthy, M.J., Kataja, M., Koponen, A.I., 2017. Experimental investigation of the flow dynamics and rheology of complex fluids in pipe flow by hybrid multi-scale velocimetry. Exp. Fluid 58, 158. https://doi.org/10.1007/s00348-017-2440-9.

Hao, L., Mellor, S., Seaman, O., Henderson, J., Sewell, N., Sloan, M., 2010. Material characterisation and process development for chocolate additive layer manufacturing. Virtual Phys. Prototyp. 5, 57–64. https://doi.org/10.1080/17452751003753212.

He, Y., Yang, F., Zhao, H., Gao, Q., Xia, B., Fu, J., 2016. Research on the printability of hydrogels in 3D bioprinting. Sci. Rep. 6, 29977 https://doi.org/10.1038/srep29977.

Le Tohic, C., O'Sullivan, J.J., Drapala, K.P., Chartrin, V., Chan, T., Morrison, A.P., Kerry, J.P., Kelly, A.L., 2018. Effect of 3D printing on the structure and textural properties of processed cheese. J. Food Eng. 3D Print. Food – Des. Technol. 220, 56–64. https://doi.org/10.1016/j.jfoodeng.2017.02.003.

Le-Bail, A., Maniglia, B.C., Le-Bail, P., 2020. Recent advances and future perspective in additive manufacturing of foods based on 3D printing. Curr. Opin. Food Sci. Food Eng. Process. 35, 54–64. https://doi.org/10.1016/j.cofs.2020.01.009.

Liu, Q., Zhang, N., Wei, W., Hu, X., Tan, Y., Yu, Y., Deng, Y., Bi, C., Zhang, L., Zhang, H., 2020a. Assessing the dynamic extrusion-based 3D printing process for power-law fluid using numerical simulation. J. Food Eng. 275, 109861 https://doi.org/10.1016/j.jfoodeng.2019.109861.

Liu, Y., Yu, Y., Liu, C., Regenstein, J.M., Liu, X., Zhou, P., 2019a. Rheological and mechanical behavior of milk protein composite gel for extrusion-based 3D food printing. LWT 102, 338–346. https://doi.org/10.1016/j.lwt.2018.12.053.

Liu, Z., Bhandari, B., Prakash, S., Mantihal, S., Zhang, M., 2019b. Linking rheology and printability of a multicomponent gel system of carrageenan-xanthan-starch in extrusion based additive manufacturing. Food Hydrocolloids 87, 413–424. https://doi.org/10.1016/j.foodhyd.2018.08.026.

Liu, Z., Dick, A., Prakash, S., Bhandari, B., Zhang, M., 2020b. Texture modification of 3D printed air-fried potato snack by varying its internal structure with the potential to reduce oil content. Food Bioprocess Technol. 13, 564–576. https://doi.org/10.1007/s11947-020-02408-x.

Lucas, B.D., Kanade, T., 1981. An iterative image registration technique with an application to stereo. Vision 81, 674–679.

Ma, Y., Schutyser, M.A.I., Boom, R.M., Zhang, L., 2021. Predicting the extrudability of complex food materials during 3D printing based on image analysis and gray-box data-driven modelling. Innovat. Food Sci. Emerg. Technol. 73, 102764 https://doi.org/10.1016/j.ifset.2021.102764.

Moetazedian, A., Budisuharto, A.S., Silberschmidt, V.V., Gleadall, A., 2020. CONVEX (CONtinuously Varied EXtrusion): a new scale of design for additive manufacturing. Addit. Manuf. 101576. https://doi.org/10.1016/j.addma.2020.101576.

Montoya, J., Medina, J., Molina, A., Gutiérrez, J., Rodríguez, B., Marín, R., 2021. Impact of viscoelastic and structural properties from starch-mango and starch-arabinoxylans hydrocolloids in 3D food printing. Addit. Manuf. 39, 101891 https://doi.org/10.1016/j.addma.2021.101891.

Moretti, M., Rossi, A., Senin, N., 2021. In-process simulation of the extrusion to support optimisation and real-time monitoring in fused filament fabrication. Addit. Manuf. 38, 101817 https://doi.org/10.1016/j.addma.2020.101817.

Nijdam, J.J., Agarwal, D., Schon, B.S., 2021. An experimental assessment of filament-extrusion models used in slicer software for 3D food-printing applications. J. Food Eng. 110711 https://doi.org/10.1016/j.jfoodeng.2021.110711.

Nuchitprasitchai, S., Roggemann, M., Pearce, J.M., 2017. Factors effecting real-time optical monitoring of fused filament 3D printing. Prog. Addit. Manuf. 2, 133–149. https://doi.org/10.1007/s40964-017-0027-x.

Ross, M.M., Crowley, S.V., Crotty, S., Oliveira, J., Morrison, A.P., Kelly, A.L., 2021. Parameters affecting the printability of 3D-printed processed cheese. Innovat. Food Sci. Emerg. Technol. 72, 102730 https://doi.org/10.1016/j.ifset.2021.102730.

Schutyser, M.A.I., Houlder, S., de Wit, M., Buijsse, C.A.P., Alting, A.C., 2018. Fused deposition modelling of sodium caseinate dispersions. J. Food Eng. 3D Print. Food – Des. Technol. 220, 49–55. https://doi.org/10.1016/j.jfoodeng.2017.02.004.

Serdeczny, M.P., Comminal, R., Mollah, MdT., Pedersen, D.B., Spangenberg, J., 2020a. Numerical modeling of the polymer flow through the hot-end in filament-based material extrusion additive manufacturing. Addit. Manuf. 36, 101454 https://doi.org/10.1016/j.addma.2020.101454.

Serdeczny, M.P., Comminal, R., Pedersen, D.B., Spangenberg, J., 2020b. Experimental and analytical study of the polymer melt flow through the hot-end in material extrusion additive manufacturing. Addit. Manuf. 32, 100997 https://doi.org/10.1016/j.addma.2019.100997.

Siacor, F.D.C., Chen, Q., Zhao, J.Y., Han, L., Valino, A.D., Taboada, E.B., Caldona, E.B., Advincula, R.C., 2021. On the additive manufacturing (3D printing) of viscoelastic materials and flow behavior: from composites to food manufacturing. Addit. Manuf. 45, 102043 https://doi.org/10.1016/j.addma.2021.102043.

Sombatsompop, N., Dangtangee, R., 2002. Effects of the actual diameters and diameter ratios of barrels and dies on the elastic swell and entrance pressure drop of natural rubber in capillary die flow. J. Appl. Polym. Sci. 86, 1762–1772. https://doi.org/10.1002/app.11212.

Sridharan, S., Meinders, M.B.J., Sagis, L.M., Bitter, J.H., Nikiforidis, C.V., 2021. Jammed emulsions with adhesive pea protein particles for elastoplastic edible 3D printed materials. Adv. Funct. Mater. n/a 2101749. https://doi.org/10.1002/adfm.202101749.

Sun, Y., Zhang, M., Chen, H., 2020. LF-NMR intelligent evaluation of rheology and printability for 3D printing of cookie dough pretreated by microwave. LWT 132, 109752. https://doi.org/10.1016/j.lwt.2020.109752.

Teng, X., Zhang, M., Mujumdar, A.S., 2021. 4D printing: recent advances and proposals in the food sector. Trends Food Sci. Technol. 110, 349–363. https://doi.org/10.1016/j.tifs.2021.01.076.

Tian, X., Li, Y., Ma, D., Han, J., Xia, L., 2021. Closed-loop control of silicone extrusion-based additive manufacturing based on machine vision. In: Presented at the ASME 2021 16th International manufacturing Science and Engineering Conference, American Society of Mechanical Engineers Digital Collection. https://doi.org/10.1115/MSEC2021-63719.

Vancauwenberghe, V., Katalagarianakis, L., Wang, Z., Meerts, M., Hertog, M., Verboven, P., Moldenaers, P., Hendrickx, M.E., Lammertyn, J., Nicolaï, B., 2017. Pectin based food-ink formulations for 3-D printing of customizable porous food simulants. Innovat. Food Sci. Emerg. Technol. 42, 138–150. https://doi.org/10.1016/j.ifset.2017.06.011.

Wegrzyn, T.F., Golding, M., Archer, R.H., 2012. Food Layered Manufacture: a new process for constructing solid foods. Trends Food Sci. Technol. 27, 66–72. https://doi.org/10.1016/j.tifs.2012.04.006.

Wu, P., Ramani, K.S., Okwudire, C.E., 2021. Accurate linear and nonlinear model-based feedforward deposition control for material extrusion additive manufacturing. Addit. Manuf. 48, 102389 https://doi.org/10.1016/j.addma.2021.102389.

Xia, H., Lu, J., Dabiri, S., Tryggvason, G., 2018. Fully resolved numerical simulations of fused deposition modeling. Part I: fluid flow. Rapid Prototyp. J. 24, 463–476. https://doi.org/10.1108/RPJ-12-2016-0217.

Zhang, L., Versteege, S., Alting, A.C., Schutyser, M.A., 2020. Impact of conjugation with maltodextrin on rheological properties of sodium caseinate. Int. Dairy J. 105, 104660 https://doi.org/10.1016/j.idairyj.2020.104660.

Zhu, S., Ribberink, M., de Wit, M., Schutyser, M., Stieger, M., 2020. Modifying sensory perception of chocolate coated rice waffles through bite-to-bite contrast: an application case study using 3D inkjet printing. Food Funct. 11, 10580–10587. https://doi.org/10.1039/d0fo01787f.

Zhu, S., Ruiz de Azua, I.V., Feijen, S., van der Goot, A.J., Schutyser, M., Stieger, M., 2021. How macroscopic structure of 3D printed protein bars filled with chocolate influences instrumental and sensory texture. LWT 151, 112155. https://doi.org/10.1016/j.lwt.2021.112155.

Zhu, S., Stieger, M.A., van der Goot, A.J., Schutyser, M.A.I., 2019. Extrusion-based 3D printing of food pastes: correlating rheological properties with printing behaviour. Innovat. Food Sci. Emerg. Technol. 58, 102214 https://doi.org/10.1016/j.ifset.2019.102214.